Soft Matter

PAPER

View Article Online
View Journal | View Issue

Cite this: *Soft Matter*, 2014, **10**, 8031

Chemoenvironmental modulators of fluidity in the suspended biological cell†

John M. Maloney[a] and Krystyn J. Van Vliet*[b]

Biological cells can be characterized as "soft matter" with mechanical characteristics potentially modulated by external cues such as pharmaceutical dosage or fever temperature. Further, quantifying the effects of chemical and physical stimuli on a cell's mechanical response informs models of living cells as complex materials. Here, we investigate the mechanical behavior of single biological cells in terms of fluidity, or mechanical hysteresivity normalized to the extremes of an elastic solid or a viscous liquid. This parameter, which complements stiffness when describing whole-cell viscoelastic response, can be determined for a suspended cell within subsecond times. Questions remain, however, about the origin of fluidity as a conserved parameter across timescales, the physical interpretation of its magnitude, and its potential use for high-throughput sorting and separation of interesting cells by mechanical means. Therefore, we exposed suspended CH27 lymphoma cells to various chemoenvironmental conditions—temperature, pharmacological agents, pH, and osmolarity—and measured cell fluidity with a non-contact technique to extend familiarity with suspended-cell mechanics in the context of both soft-matter physics and mechanical flow cytometry development. The actin-cytoskeleton-disassembling drug latrunculin exacted a large effect on mechanical behavior, amenable to dose-dependence analysis of coupled changes in fluidity and stiffness. Fluidity was minimally affected by pH changes from 6.5 to 8.5, but strongly modulated by osmotic challenge to the cell, where the range spanned halfway from solid to liquid behavior. Together, these results support the interpretation of fluidity as a reciprocal friction within the actin cytoskeleton, with implications both for cytoskeletal models and for expectations when separating interesting cell subpopulations by mechanical means in the suspended state.

Received 4th April 2014
Accepted 13th August 2014

DOI: 10.1039/c4sm00743c

www.rsc.org/softmatter

I. Introduction

The mechanical response of a single biological cell is increasingly well understood in terms of viscoelastic parameters, though the mechanistic origins of these quantities remain unclear. A map of deformation regimes (Fig. 1) is useful, whether one wants to investigate the biophysical nature of the eukaryotic cell as a type of animate "soft matter",[1,2] or to leverage mechanical traits in practical applications such as high-throughput mechanical flow cytometry and the separation of relevant subpopulations for therapeutic purposes.[3–5] Around a timescale of 1 s, and for strains of up to at least 100%, cells obey so-called power-law rheology (also described as constant-phase or fractional-derivative rheology).[6–14] Up to a threshold of nonlinearity corresponding to a strain rate of $\lesssim 1\%\ s^{-1}$,[15,16] whole cells are well described mechanically by two parameters:

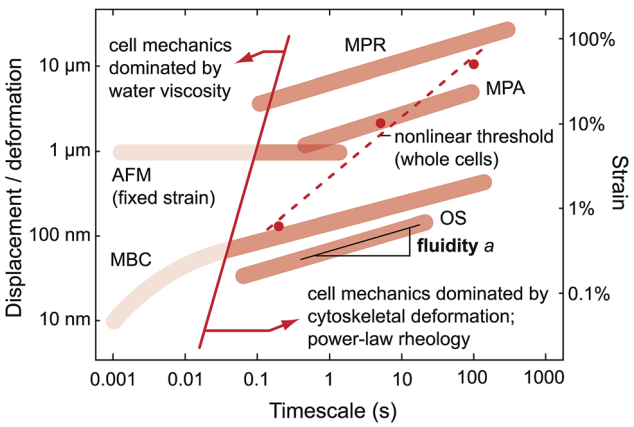

Fig. 1 Deformation regime map for biological cells around 1 s. Slanted darker regions denote findings of power-law rheology (log–log slope of fluidity *a* when load is fixed) by various techniques. Dotted line connects reported threshold points of nonlinear load-displacement relationship for whole cells.[15,16] At much shorter timescales, water viscosity dominates mechanical response; lighter regions denote findings of the transition between regimes. Selected large-timescale-range reports: MPR = microplate rheometry,[8,9] MPA = micropipette aspiration,[13] AFM = atomic force microscopy,[14] MBC = magnetic bead cytometry,[6] OS = optical stretching.[17]

[a]*Department of Materials Science and Engineering, Massachusetts Institute of Technology, 77 Massachusetts Avenue, Cambridge, MA 02139, USA. E-mail: krystyn@mit.edu*

[b]*Department of Materials Science and Engineering and Department of Biological Engineering, Massachusetts Institute of Technology, Cambridge, MA 02139, USA*

† Electronic supplementary information (ESI) available. See DOI: 10.1039/c4sm00743c

a stiffness, representing the load amplitude required to obtain a given deformation amplitude in oscillatory testing; and a frequency-independent fluidity that represents the phase lag between load and deformation sinusoids, normalized to the extremes of an elastic solid and a viscous liquid.[17] Fig. 1 highlights the findings of measurement approaches capable of spanning a wide range of time scales, a crucial capability for detecting the conditions under which power-law rheology dominates as a deformation mechanism.

We focus on fluidity of individual cells for several reasons. First, fluidity a is arguably the predominant descriptive parameter of cell mechanics around 1 s: it is conserved across decades of frequency around this timescale;[9,18] it also governs, as the power-law exponent, both the angular frequency dependence of complex modulus as $G^*(\omega) \propto (i\omega)^a$ and the time dependence of creep compliance as $J(t) \propto t^a$.[9,19] Second, nondimensional fluidity ranges from 0 (solid) to 1 (fluid) and is relatively easy to compare across multiple cytorheological techniques, as tool-specific models of load-displacement coupling are not required. While fluidity can be extracted from the power-law stiffness-frequency[6,11] or deformation-time[7,8] relationships, it can also be obtained independently from oscillatory phase lag.[9,18] Third, fluidity may be useful in separating cell (sub)populations as a complement to stiffness, which exhibits a large, right-skewed distribution[6–9,11,20–22] that hinders error-free sorting by mechanical means. An understanding of intrinsic cell-to-cell heterogeneity of fluidity and stiffness, and the relationship between distribution shape and size of these two parameters,[23,24] could improve the accuracy of mechanical flow cytometry techniques and provide insight into the origins of cell-to-cell mechanical dispersion.

However, the mechanisms responsible for cell fluidity have been challenging to identify. Prominent models of power-law rheology in inanimate materials have related the magnitude of fluidity a (equivalently, the power-law exponent) to a noise temperature $x = a + 1$ that quantifies athermal agitation as a driving force for rearrangement.[6,19,25] (This noise temperature is analogous to thermodynamic temperature; it governs the likelihood of structural rearrangement *via* a Boltzmann relationship, but is—in theory—dominated by rearrangement-driven agitation from neighboring regions rather than thermal energy.) Alternatively, they have related the reciprocal of fluidity to the height of energy barriers impeding relaxation.[26] The crucial prediction of these models is a broad distribution of relaxation times that in cells is associated with the range of cytoskeletal length scales, including filament segment length and crosslink spacing, that precludes accurate representation of cell mechanics over a large frequency range by one or several spring–dashpot pairs.[6,9,10,12,17] Still lacking, however, is a direct understanding of the molecular origin of the magnitude of fluidity and its modulation by various chemoenvironmental factors, especially when measured independently of stiffness. Therefore, the primary goal of the current work is to add experimental findings that enable new models or extension of existing models to describe how fluidity of suspended cells is modulated by temperature, cytoskeleton (dis)assembly, pH, and osmotic pressure.

Oscillatory optical stretching (OOS) is a well-suited approach to investigate the linear power-law regime of suspended biological cells, including tracking fluidity as a function of chemoenvironmental condition. Optical stretching, which deforms cells without physical contact, also uncouples cell mechanics from cell size and stickiness, factors that can complicate interpretation in characterization tools that squeeze cells with intrinsically disperse sizes between posts or through channels of fixed size. With the capability of measuring ~10 nm deformations of fully suspended cells, optical stretching can identify whether attached-cell conclusions still hold. Fluidity is an especially convenient parameter to measure by this tool because unlike stiffness, it does not depend on cell refractive index, which can vary among cells.[27] After earlier demonstration showing equivalence between parameters obtained in the time and frequency domains,[17] we exclusively use the frequency domain to maximize the number of cells analyzed per condition. The advantages of using oscillatory loads to quantify the effects of chemical and physical perturbations are that they (1) avoid having to discard consideration of cells that rotate during creep compliance experiments;[28] (2) minimize analysis complications arising from temperature transients when laser power is increased suddenly;[17,28] and (3) enable subsecond determination of fluidity (shown herein). We previously showed that the magnitude and temperature dependence of fluidity is essentially identical between adherent primary human mesenchymal stem cells, adherent immortalized fibroblasts, and suspended immortalized lymphoma cells;[17] here, we analyze a wide range of chemoenvironmental conditions applied to the same suspended cell line (CH27 lymphoma). We also take advantage of the capability of the optical stretcher to heat cells to near-physiological temperature during mechanical interrogation.

We here report the degree of fluidity modulation over the first 1–2 hours after a chemoenvironmental change, to clarify which notable effects persist in the suspended state, to expand the experimental space available when reconciling models of cell rheology, and to further the development of mechanical cytometry techniques. The chemoenvironmental space is explored by changing temperature with laser power, by pharmacological challenges, by extracellular and intracellular pH control, and by changing the osmotic pressure in extracellular media. We emphasize accompanying mechanical and dose dependence parameters with estimated error or confidence interval, as calculated by bootstrapping. This analysis of cell fluidity under a wide range of perturbations, and with quantified considerations of uncertainty, affords insight into why such perturbations alter (or leave unchanged) the mechanical fluidity of suspended cells, as can be useful for mechanical cytometry; and also provides insight into a physical interpretation of fluidity. The results are most clearly understood, we suggest, by viewing whole-cell fluidity as a mean reciprocal or inverse friction within the actin-based cytoskeleton during deformation and rearrangement.

II. Materials and methods

Cell culture and preparation

Murine CH27 lymphoma cells[29] were obtained courtesy of D. J. Irvine (MIT) and cultured in RPMI (Gibco #11875) with 10%

fetal bovine serum (Atlanta Biologicals #S11550). Cell size (specifically, suspended cell diameter) was found by optical microscopy to be log-normally distributed with a median diameter of 17.6 μm and a geometric standard deviation of 1.09.

Population refractive index was measured by immersion refractometry,[27,30] in which the refractive index of extracellular media is adjusted until cells appear transparent by phase contrast microscopy. A bovine serum albumin (BSA) solution of approximately 0.4 g mL^{-1} was prepared, and cell-media suspensions were centrifuged and resuspended in 0.5 mL of this stock solution with an equal amount set aside without cells. Water (in 25, 50, or 100 μL amounts) was successively added to each sample, followed each time by removal of 50 μL from the cell preparation for photography and 50 μL from the cell-free sample for refractive index measurement (Refracto 30PX). Typical appearance of cells is shown in Fig. 5(c).

DMSO was generally used for solubilizing drugs in 100–1000× stock solutions before delivery to cells; in agreement with a previous report,[13] we confirmed that up to 1% DMSO does not detectably alter stiffness (64.4 ± 1.5 Pa *vs.* 64.7 ± 4 Pa with DMSO) or fluidity (0.243 ± 0.004 *vs.* 0.26 ± 0.01 with DMSO), for 5 Hz testing at 37 °C. In drug experiments, stock solutions were prepared of latrunculin A (Millipore #428026, 1 mM in DMSO, to bind actin monomers and drive filamentous actin depolymerization); compositions of other drug solutions are given in ESI.†

In pH experiments, cells were exposed either to sodium-bicarbonate-free DMEM with pH adjusted to 6.5–8.5 by HCl and/or NaOH, or to the nigericin-K^+ clamp protocol[31] consisting of 10 μM nigericin (Sigma #N7143, used in a 1000× stock solution in ethanol) and a suspension medium of 140 mM $K_2H_2PO_4$ and 10 mM NaCl.

To osmotically challenge cells, cell suspensions were mixed with deionized water or 1 M sucrose in phosphate-buffered saline (PBS). For CH27 cells, the ion channel blockers NPPB (Santa Cruz Biotechnology #sc-201542, 200 μM, from 50 mM stock solution in DMSO) and DCPIB (Santa Cruz Biotechnology #sc-203913, 50 μM, from 50 mM stock solution in DMSO) both were needed during hypotonic environments to block regulatory volume decrease that would otherwise return the cells to approximately normal size within tens of minutes.[32] In hypertonic environments, use of the ion channel blocker EIPA (Santa Cruz Biotechnology #sc-202458, 50 μM, from 25 mM stock solution in DMSO) was explored[32] but was not necessary to maintain a shrunken state for at least one hour of optical stretching (Table SI in ESI†). The extent of testable hypotonicity was limited by the suppressed refractive index inside the swollen cell, which reduces the photon-stress coupling in optical stretching and consequently reduces oscillatory deformation below the noise limit. The extent of testable hypertonicity was limited by the tendency of cells to shrink into non-spherical shapes that tended to spin irregularly during optical stretching, complicating image analysis.

Microfluidic optical stretching

Oscillatory optical stretching and subsequent data analysis in the frequency domain were conducted based on the optical stretching concept developed by Guck *et al.*,[33] a chamber design developed by Lincoln and Guck *et al.*,[34] and an oscillatory analysis reported previously by us.[17] Briefly, suspended CH27 cells were diluted to a convenient density of 100 K mL^{-1}, which provides favorably tight cell-to-cell spacing along the flow channel to increase throughput without clumping. They were then injected, *via* a syringe and microfluidic tubing, into a hollow glass capillary positioned between two optical fibers (Fig. 2(a)) and serially exposed to two counterpropagating 1064 nm laser beams. The laser beams followed a sinusoidal profile for 8 s with a mean power of 0.7 W per fiber (unless otherwise specified) and a load amplitude of 0.5 W per fiber (*i.e.*, 1 W peak-to-peak per fiber). Simultaneously, cell images were recorded by phase contrast microscopy at 50 frames s^{-1}.

Deformation was characterized by the edge-to-edge distance, along the laser axis, of a phase-contrast image of the cell, normalized to the distance measured during a brief 0.2 W per fiber trapping period. In the current study this deformation was ~0.2% of the cell diameter. The photonic surface stress on a cell at the center of the beam was calculated *via* previously

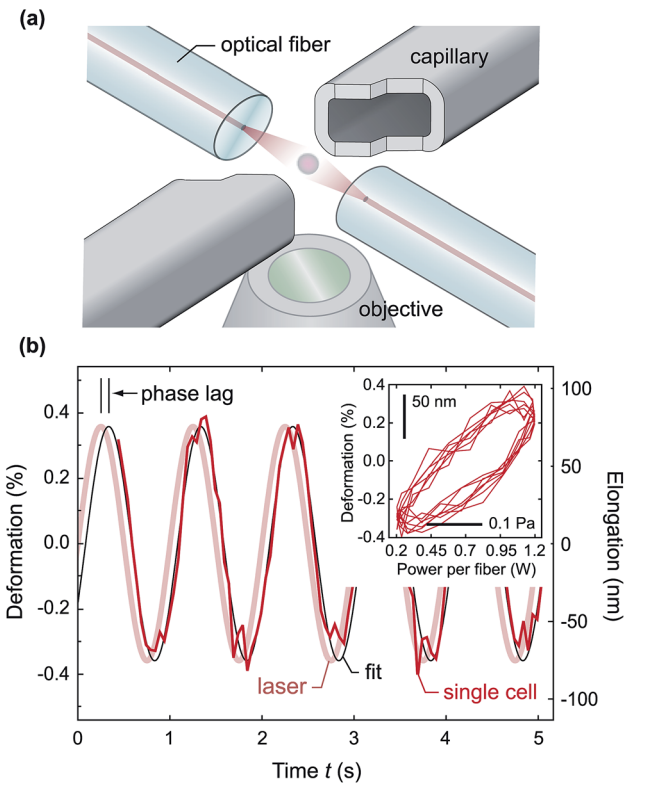

Fig. 2 (a) Optical stretching (OS) in the frequency domain measures whole-cell mechanics in the suspended state, absent physical contact with any probe or substratum. Schematic of counterpropagating divergent laser beams directed toward a suspended cell confined within a hollow glass capillary (cutaway view shown); photonically induced deformation is characterized by the normalized elongation of the cell along the laser axis. (b) Oscillatory deformation of a single cell in response to sinusoidal loading with frequency 1 Hz. (Inset, symmetric and elliptical Lissajous figure indicates linear viscoelasticity.) The viscoelastic phase lag ϕ of the cell in radians is also a measure of cell fluidity a as $a = 2\phi/\pi$.

published models[33] to equal 0.258 Pa per 1 W laser power per fiber, calculated by using previously measured fiber distances and chamber geometry,[17] and a measured average refractive index of CH27 cells of 1.375. The unfocused beams had a $1/e^2$ diameter of 31 μm and a divergence angle of 0.15 μm per 1 μm of additional distance from the fiber end, which lay approximately 200 μm away.[17] Cells with a size distribution of 10% around a median diameter of 17–18 μm were considerably narrower than the beam and far from its source, and thus exposed to a surface stress that was minimally coupled to cell size. Amplitudes and phase angles were extracted from deformation signals by subtracting a moving average across one or more periods and fitting the expression $F\sin[\omega(t - t_0) - \phi]$ by nonlinear regression (Mathematica, Wolfram Research) where F is the deformation amplitude, ω is the applied angular frequency, t_0 is the measured lag of the tool (collection, processing, and transmission time of laser data and image frames[17]) and ϕ is the phase angle representing whole-cell hysteresivity. Stiffness in the form of complex modulus magnitude $|G^*(\omega)|$ was then calculated by dividing photonic stress by deformation amplitude; fluidity a, corresponding to whole-cell hysteresis or damping, was calculated as $a = 2\phi/\pi$.

The signal-to-noise ratio (SNR) is the mean-squared magnitude of the fitted sinusoid divided by the mean-squared magnitude of the flattened deformation with the signal subtracted. Cells with SNR < 1 (4% of cells at 0.7 W per fiber mean, 0.5 W per fiber amplitude, 5 Hz) were excluded because misfitted fluidity values of $a < 0$ or $a > 1$ became much more likely below this threshold. (Signal strength can be increased by testing at a larger mean or amplitude power or by decreasing frequency.)

In optical stretching, laser beam absorption increases the temperature of the cell and surrounding medium. Temperature changes within microscale volumes were characterized by using the fluorescent dye Rhodamine B, the brightness of which is attenuated by 1.69% $^\circ C^{-1}$ above room temperature $T_\infty = 20 \pm 1$ °C.[17] Dye brightness was insensitive to focal plane height, photobleaching was negligible when the dye was illuminated for several seconds only, and background fluorescent signal was easily measured by flushing dye from the capillary. As a result, it was not necessary to use a reference dye such as Rhodamine 110. The temperature step response at incident laser power P follows $T(t) = T_\infty + C_1P\ln(1 + C_2t)$, where $C_1 = 1.17\ ^\circ C\ W^{-1}$ and $C_2 = 5700\ s^{-1}$ are constants representing the geometry and thermal characteristics of the system.[17] This form can be used, by convolution with an input laser profile, to estimate the average temperature increase of 23–24 °C per W per fiber during 8 s of stretching when preceded by several seconds of low-power (0.2 W per fiber) trapping. Heating from room temperature to physiological temperature can therefore be accomplished at a power of 0.7 W per fiber, as discussed in the main text.

Data analysis

Error bars in all figures show standard error. When extracting fluidity from deformation signals, nonlinear regression error, shown in Fig. 4(c), was calculated as $[\mathrm{MSE}(\mathbf{D}'\mathbf{D})^{-1}]^{1/2}$ where MSE is the mean squared error (the sum of squared residuals divided by the number of degrees of freedom) and $\mathbf{D}$ is the matrix of partial derivatives of the model evaluated at the final estimates.[35]

Fluidity and stiffness were treated as normally and lognormally distributed parameters, respectively, based on our observation of the data and an abundance of reports.[6–9,11,20–22] Population averages therefore represent arithmetic and geometric means, respectively. The error in fitted parameters such as half-maximal concentration and frequency-stiffness invariant point was estimated by using the statistical technique of bootstrapping, or resampling with replacement, as discussed previously.[28,36]

In pharmacological experiments, an iterative approach was used to estimate a unified median (half-maximal) dose C_{50} from paired changes in fluidity and stiffness. First, a first-order dependence was assumed for (normally distributed) fluidity a and (log-normally distributed) stiffness G on drug concentration C, based on the appearance of the data:

$$a(C) = a_{\mathrm{saturation}} + \frac{a_{\mathrm{saturation}} - a_{\mathrm{baseline}}}{C/C_{50} + 1};$$

$$\ln G(C) = [\ln(G)]_{\mathrm{saturation}} + \frac{[\ln(G)]_{\mathrm{saturation}} - [\ln(G)]_{\mathrm{baseline}}}{C/C_{50} + 1}.$$

By using an initial guess for C_{50}, baseline and saturation parameters were fit to the existing data consisting of concentration-fluidity pairs of values for all cells. Second, these four parameters were used to normalize all experimental values, which were then averaged together to represent a unified function of concentration that varied from 0 to 1 with increasing dose. Third, a new C_{50} value was obtained by fitting to this unified function, and the process was repeated to convergence. Following convergence, bootstrapping of the $2N$ normalized values—normalized a *vs.* C and normalized $\ln(G)$ *vs.* C points—was used to obtain the 95% confidence interval of the median concentration (which itself followed a lognormal distribution). Here, for simplicity, values of the sigmoidal dose-dependence model were calculated at discrete points and the extreme 5% of parameter values were excluded to create a 95% confidence band, as shown in Fig. 5(a and b). This approach incorporates all available fluidity and stiffness data to identify key concentration-related parameter(s) from pharmacological modulation.

The soft glassy rheology model describes an invariant point (ω_{inv}, G_{inv}) that applies to materials exhibiting power-law rheology.[25] This model represents deformation in a certain class of materials as activation of a broad spectrum of energy wells. Each energy well has characteristic depth E and activation time $\tau = \exp(E/x)$, with normalized postulated distribution $P_{\mathrm{eq}}(E) = [(x - 1)/x]\exp(E/x)\exp(-E)$ and where $x = a + 1$ is the nondimensional noise temperature that characterizes agitation. The complex modulus in the linear regime is

$$G^*(\omega) \propto \int_1^\infty P_{eq}(\tau)\left(\frac{i\omega\tau}{\omega_{inv} + i\omega\tau}\right)d\tau,$$

where $P_{eq}(\tau)$ is calculated as $|dE/d\tau|P_{eq}(E) = (x-1)\tau^{-x}$. Integration and assumption of small ω gives $G \propto \Gamma(1+a)\Gamma(1-a)(i\omega)^a$, and so measured stiffness $|G^*|$ values should be divided by $\Gamma(1+a)\Gamma(1-a)$ before performing the pivoting analysis. Previous analyses have instead often performed pivoting analysis by using the storage modulus $G' = |G^*|\cos(\pi a/2)$,[6,21,24,37] achieving a similar result (*i.e.*, $\cos(\pi a/2) \approx [\Gamma(1+a)\Gamma(1-a)]^{-1}$). We follow this approach to enable simple comparison between reports; correction instead by using the gamma terms increases our estimate of $\omega_{inv} = 4.8$ kHz by 31%, a relatively small change compared to the uncertainty of ω_{inv}.

The invariant point (ω_{inv}, G_{inv}) is, in the soft glassy rheology model, the common intersection of lines describing the relationship between stiffness *vs.* frequency in the log-transformed domain (Fig. 5(e)). The slope of a line corresponds to a fluidity value measured under a certain condition. Chemo-environmental modulation, including drug dosing, causes pivoting around this point as stiffness and fluidity change in concert (Fig. 5(a and b)). Note that when >2 lines are obtained through experiment, they will generally not meet at a single point. Therefore, a least-squares approach was used to estimate the best intersection point; its uncertainty, in the form of a 95% confidence region, was determined *via* bootstrapping. The details of this analysis are given in ESI, Fig. S1.†

III. Results and discussion

Frequency-domain optical stretching enables subsecond fluidity measurements at physiological temperatures

We conducted oscillatory rheological tests of fully suspended CH27 lymphoma cells to examine initially their viscoelastic properties at different temperatures and oscillation frequencies; a range of input laser powers and excitation frequencies served to explore the spectrum of responses and to identify useful tool settings for further experiments. Fluidity increases with increasing cell temperature, a function of incident laser power;[17] now with improved data density near 37 °C, we find the associated rate to be 0.013 °C^{-1} with 95% confidence interval [0.011, 0.015] °C^{-1} (Fig. 3(a)). (To be clear, the temperature increase is caused entirely by infrared laser irradiation sustained over several seconds of cell stretching, and thus any measured fluidity change represents a near-instantaneous change in whole-cell rheology. In anticipation of later discussion of fluidity *vs.* cell volume, we note also that no volumetric changes occurred over this timescale (Fig. S2 in ESI†).) Note that it is possible to probe cells near physiological temperature by careful selection of laser power (0.7 W per fiber in our chamber); that is, cells are loaded into the optical stretcher at room temperature and heated to a mean temperature of 37 °C during stretching. We next investigated the temperature excursion around the mean value at different laser oscillation frequencies. As shown in Fig. 3(b), temperature oscillation amplitude was attenuated with increasing frequency. (At sufficiently high frequencies, conduction to neighboring regions is minimal,

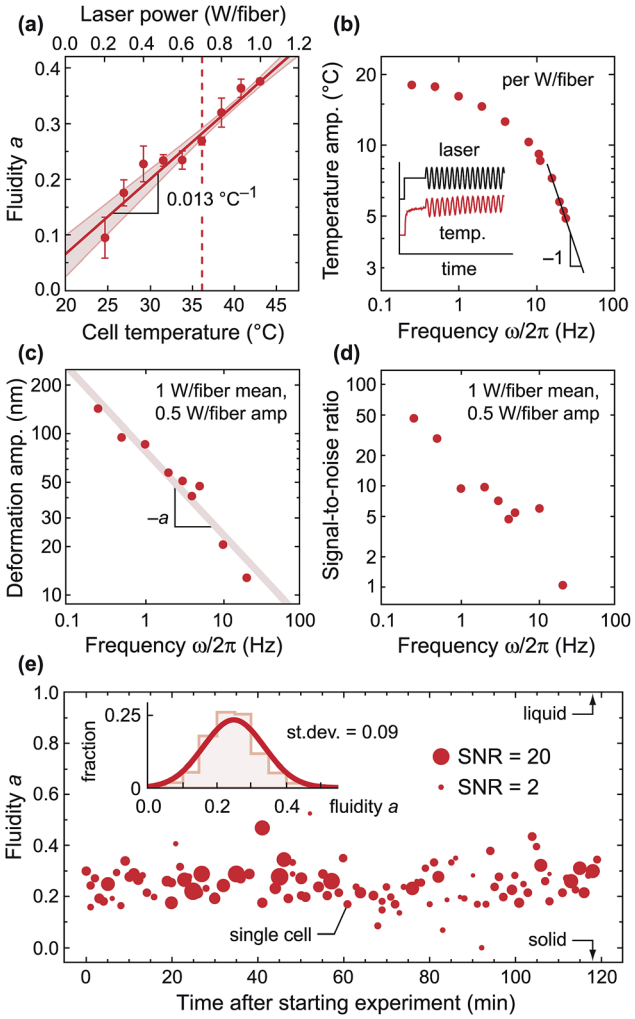

Fig. 3 Optical stretching settings can be adjusted to maintain near-physiological temperature while producing measurable deformation. (a) Fluidity of CH27 lymphoma cells increases with temperature at a rate of 0.013 °C^{-1} (lighter band shows 95% confidence interval). Dotted line shows mean laser power selection of 0.7 W per fiber to bring the cell to physiological temperature during stretching. (b) Temperature excursions around the mean temperature are attenuated with increasing load angular frequency ω, converging to $\Delta T(\omega) \propto \omega^{-1}$ behavior as ω increases. (Inset, example of amplitude characterization as determined by temperature-dependent fluorescent dye.) (c) Whole-cell deformation amplitude decreases with increasing angular frequency as ω^{-a} over the power-law regime; in turn, (d) median signal-to-noise ratio (SNR) also decreases. (e) With parameter selection of 0.7 W per fiber mean laser power and 5 Hz frequency, fluidity is stable and signal strength is suitably strong over a duration of two hours. (Inset, Gaussian distribution of fluidity values.)

and the temperature-frequency relationship follows a slope of −1 on a log–log scale, corresponding to lumped-capacitance heating of the irradiated area only.)

A desire to minimize excess heating of the cell (and to identify phase lag quickly) therefore motivates maximizing the frequency when performing oscillatory optical stretching on cells. However, a disadvantage of using higher frequencies is the concomitant attenuation of deformation, which follows a

power law that depends upon fluidity a as $\propto \omega^{-a}$ (Fig. 3(c)). In turn, the signal-to-noise ratio (SNR) of deformation also decreases (Fig. 3(d)). As a compromise between more rapid *vs.* more reliable characterization while maintaining near-physiological temperature, we selected a mean power of 0.7 W per fiber (0.5 W per fiber amplitude) and a frequency of 5 Hz for the remainder of the experiments presented here. Shown in Fig. 3(e) are data from 107 cells over a two-hour experiment performed at these settings; each cell provided a single value of fluidity, a unitless quantity that varies in theory between 0 and 1. Fluidity magnitudes were essentially constant over this two-hour duration, with a mean of 0.242 ± 0.007 and with individual cells exhibiting suitably large SNR values. The signal strength (SNR) further appeared independent of large or small fluidity magnitudes (Fig. S3 in ESI†). We found the intrinsic cell-to-cell variation in fluidity (measured as standard deviation of the near-Gaussian distribution) to be 0.07 for this collection of cells and 0.086 from the larger selection ($n = 399$, Fig. 3 (e, inset)) of all CH27 cells tested under these conditions.

How long is it necessary to stretch a certain cell to know its fluidity to a certain precision? To answer this question, we analyzed shorter oscillation periods (Fig. 4(a)) while extracting fluidity and the associated fitting error as calculated by nonlinear regression. Fig. 4(b) shows the individual-cell and population-average fluidity from a population ($n = 107$ cells) when the analysis window is reduced. Notably, this window could be reduced to well under one second with a relatively small and consistent bias, comparable to the standard error of the mean, in population fluidity; that is, although the estimated fluidity of some cells changed by >0.1, the population average was $a = 0.28 \pm 0.02$ from analyzing the first 0.25 s of oscillatory deformation data as compared to the above-noted $a = 0.24 \pm 0.01$ if all 8 s of data are analyzed. A second collection of cells ($n = 75$) produced similar results ($a = 0.30 \pm 0.02$ from a 0.25 s analysis window *vs.* $a = 0.25 \pm 0.01$ from the full 8 s window). Fig. 4(c) shows the fluidity fitting error of individual cells, as a function of analysis time. For essentially all cells, the fitting error from subsecond sampling is less than the intrinsic variation among cells. In other words, subsecond analysis of fluidity for a given cell can be attained with reasonable confidence through this approach. Note that there is no minimum measurable fluidity; even for noisy signals, one can stretch and analyze a cell over additional cycles to obtain an estimate that converges toward the true fluidity value within several seconds. To ensure that our results represent predominantly intrinsic cell-to-cell mechanical dispersion and not estimation error, we use a window of 8 s in the rest of the results described here, but emphasize based on these results that subsecond sampling is possible. Though not explored here, real-time adaptive analysis in conjunction with variable stretching times could be used to mechanically test each individual cell only as long as is necessary to reduce fitting error below an arbitrary threshold.

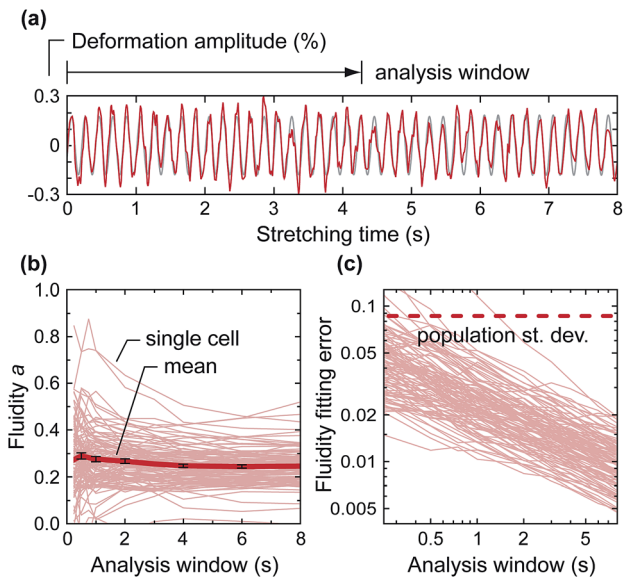

Fig. 4 (a) Fluidity can be extracted by subsecond sampling of the suspended cell, as demonstrated here by analyzing over an analysis window that includes only the beginning portion of collected time *vs.* deformation data. (b) Average fluidity is little altered even when reducing analysis window to 1 s. (c) For essentially all cells, the analysis window can be reduced to <1 s without the fitting error exceeding the intrinsic cell-to-cell variation in fluidity.

Pharmacological treatment independently alters whole-cell fluidity and stiffness

We have previously established that suspended-cell fluidity a, measured in the linear viscoelastic regime, is lowered by chemical fixation, but not detectably altered by ATP depletion.[17] As noted above, a is also increased with increasing temperature, from $a = 0.09 \pm 0.04$ at 25 °C to $a = 0.37 \pm 0.01$ at 44 °C. Here, we explore a wider range of chemoenvironmental conditions. We first consider exposing cells to select reversible pharmaceutical conditions that have been reported to alter fluidity in the attached state, and look for evidence of modulation in the suspended state in the first hour after drug application.

The strongest effect we measured was caused by the pharmacological reagent latrunculin, which binds strongly to monomeric actin and therefore induces depolymerization of filamentous actin to promote disassembly of the predominant cytoskeletal component. Fig. 5(a and b) shows the dose-dependent responses of fluidity and stiffness, which respectively increased and decreased in concert. (Latrunculin also increased cell diameter by <1 μm, Fig. S4 in ESI†.) Here, characterization of dose dependency across orders of magnitude unambiguously demonstrates pharmacological modulation while also allowing estimation of a half-maximal dose of 170 nM. The use of bootstrapping to estimate the variation in a fitted parameter provided a 95% confidence interval of [130, 230] nM, which encloses the equilibrium dissociation constant of 190 nM reported by Coué *et al.* for actin solutions.[38]

To relate laser-induced deformation to whole-cell stiffness, as in Fig. 5(b), it is necessary to know the coupling factor of cell refractive index.[27] We measured this parameter by immersion refractometry, finding an average value of 1.375 for CH27 cells with a standard deviation of 0.004 (Fig. 5(c)), similar to other cell types.[27] Importantly, refractive index is not detectably

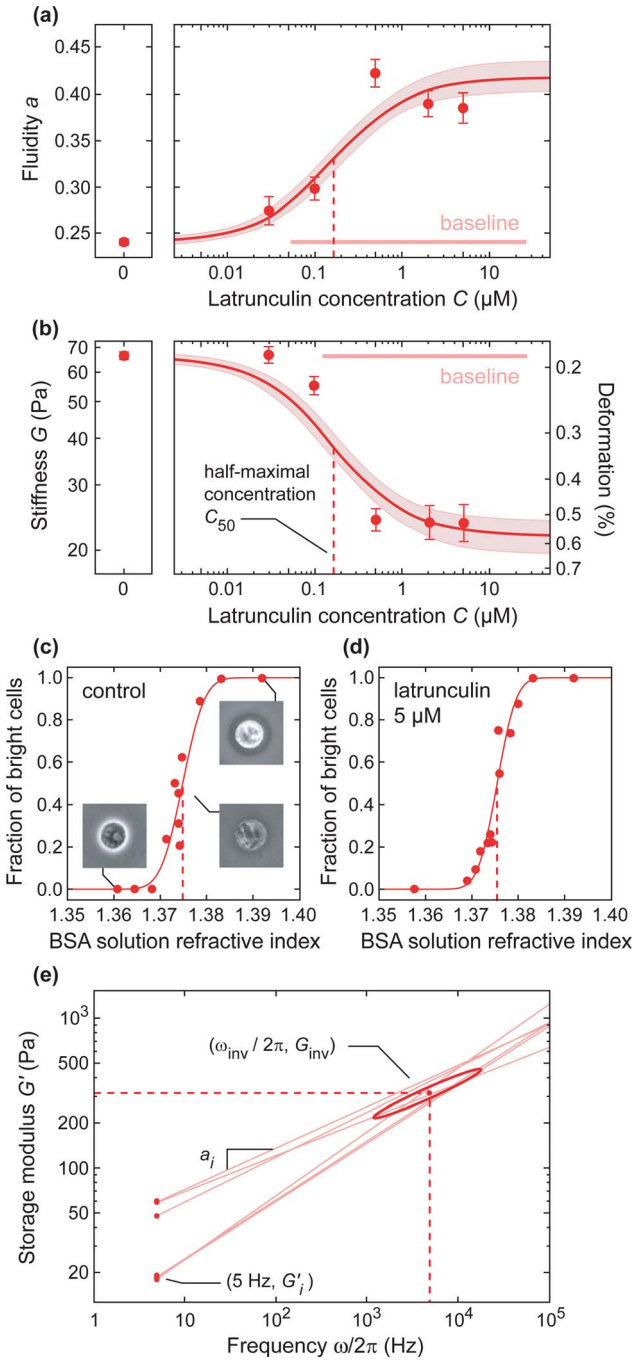

Fig. 5 (a and b) Cytoskeletal disassembly with latrunculin A increases fluidity and decreases stiffness in a dose-dependent manner with half-maximal concentration C_{50} = 170 nM (n = 30–399 cells per point, lighter band shows 95% confidence interval). (c and d) Average cell refractive index is independent of latrunculin addition. (Line shows Gaussian distribution of refractive index values with standard deviation of 0.004.) (e) Coupled fluidity-stiffness alteration with latrunculin allows identification of invariant point (ω_{inv}, G_{inv}).

altered even at the maximum latrunculin dose used in mechanical experiments (Fig. 5(d)). Stiffness and deformation measurements can therefore be shown in Fig. 5(b) to be related reciprocally. Refractive index is known to be little influenced by protein types;[30] here, we conclude that actin depolymerization and conversion from filamentous to globular form also does not alter whole-cell refractive index to a degree relevant for the photonic-mechanical coupling employed in optical stretching to quantify whole-cell fluidity and stiffness.

Coupled changes in both fluidity and stiffness upon cytoskeletal disassembly by latrunculin suggest a pivoting behavior around a single point (ω_{inv}, G_{inv}) (Fig. 5(e)).[6,25] In this interpretation, G_{inv} represents the resulting (relatively large) elastic stiffness if internal friction within the network were sufficiently large to block rearrangement and eliminate hysteresivity. The frequency represents the only characteristic time obtainable in the power-law rheology regime, the hysteresivity or fluidity being constant at other frequencies where this regime predominates. Though the collection of lines do not meet perfectly due to experimental error, it is possible to find the N-line intersection by least-squares regression, as discussed in Methods. Furthermore, the variation in the location of intersection can be estimated by bootstrapping, which produces a distribution of points that can be reshaped into a circular region by slope and scaling corrections, enclosed by a 95% confidence region that is, a region that contains 95% of the bootstrapped points, and reshaped again to be overlaid on the original plot (Fig. S1 in ESI†). The resulting 95% confidence intervals were [1.2, 17.2] kHz for $\omega_{inv}/2\pi$ and [210, 440] Pa for G_{inv}. Similar pivoting analyses have been conducted to characterize attached cells,[6,7,21,24,37,39] with a range of estimates over many orders of magnitude found by using magnetic bead cytometry and comparable values to ours ($\sim 10^4$ Hz) found by using atomic force microscopy. The connection of ω_{inv} to molecular mechanisms is therefore still unclear, and future interpretation will benefit from the accumulation of more estimates from more techniques. Note, however, that the general finding of power-law-rheology has been robust across techniques capable of examining large frequency ranges of two or more decades.[6,8,9,17,18,22]

Latrunculin A and B are well known to decrease cell stiffness by disassembling stress fibers in attached cells (*e.g.*,[40,41]), but study of latrunculin effect in suspended cells and especially on fluidity has been limited to a sample size of 5–10 cells.[42] There have been findings of increase[18,39,43] and decrease[44] in fluidity (sometimes expressed as power-law exponent a, phase lag $\pi a/2$, or noise temperature $x = a + 1$), and also of undetectable change.[42] We have attempted to resolve these differences in the context of the whole cell by using a range of doses to make the dose-dependence relationship clear and to provide a robust reference for suspended cells.

We also considered a variety of other chemical treatments intended to alter fluidity, including cholesterol insertion or extraction (to alter membrane mechanics), nocodazole and paclitaxel (to disassemble and promote, respectively, the microtubule-related cytoskeleton), acrylamide (to disassemble, in part, the intermediate-filament-related cytoskeleton), and histamine and blebbistatin (to provoke and disable actomyosin contraction, respectively). None of these treatments produced the coupled fluidity-stiffness change prominently displayed by latrunculin and amenable to dose-dependence analysis. For example, nocodazole did not detectably alter fluidity up to the

solubility limit of concentration, 33 μM (Table S1 and Fig. S5 in ESI†). Lack of detectable change from other chemicals can be attributed to a small response, undetectable at a sample size of tens of cells, for the suspended state and/or for these cells in particular compared to the detection limit of the tool, and emphasizes the impact of latrunculin and the importance of the actin cortex in dominating whole-cell response.

Osmotic challenges alter fluidity far in excess of pH changes

The next two chemoenvironmental conditions explored here were pH and tonicity. We altered intracellular pH in two ways, beginning by suspending the cells in pH-adjusted medium without buffer and performing optical stretching over the following 1–2 hours. (Intracellular pH is known to follow extracellular pH forcing to some extent over tens of minutes.[45–47]) However, we observed minimal change in mean fluidity (Fig. 6). To address the possibility of especially slow or poor coupling of pH from extra- to intracellular compartments, we ensured a matching change by using the nigericin-K^+ clamp protocol[31] to equalize intracellular and extracellular pH when potassium concentrations are also equal. Again, however, fluidity was not largely altered from its baseline value ($a = 0.24$) corresponding to testing in buffered media (pH = 7.55) with serum.

We do not rule out the possibility of small pH-dependent changes in mean fluidity around the baseline value; these could be identified, if present, by testing larger numbers of cells. The absence of a general trend agrees with conclusions from the study of actin solutions, where it was found that pH alteration over a similar range (pH 6.6 to 8.3) had a relatively small impact on filamentous actin (de)polymerization rates when compared to pharmaceutical actin monomer sequestration.[48] In cross-linked actin solutions, crosslinker identity strongly influenced the pH dependence of stiffness; in particular, the presence of fascin largely suppressed pH modulation.[49] It is evident from comparing Fig. 3(a) to Fig. 6 that in mechanical flow cytometry techniques that measure fluidity, monitoring or regulation of temperature is at least as important as that of pH.

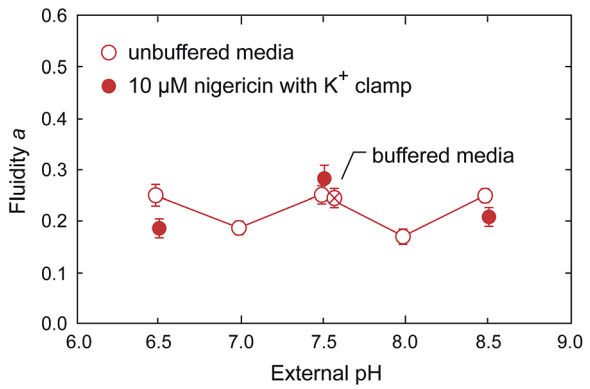

Fig. 6 Fluidity is minimally affected by pH, altered either by extracellular pH control alone or in conjunction with ionophore nigericin that equalizes intra- and extracellular pH when intra- and extracellular K^+ concentration are equalized ($n = 15–399$ cells per point).

In contrast to the effect of pH changes, osmotic challenges caused relatively large changes in fluidity, comparable to the change from latrunculin-induced cytoskeletal disassembly. Fig. 7 shows increases and decreases in fluidity for two mean laser powers with cell swelling and shrinking, respectively. Volumetric changes were accomplished by adding water or sucrose to the cell suspension along with ion channel blockers to block regulatory volume recovery (Table SII in ESI†). Notably, moving averages of cells in control conditions at each power show that even though the diameter of individual cells within the control population ranged intrinsically from 12–24 μm (with up to 14–20 μm captured here by moving average), no dependence of fluidity on cell size was detected in the absence of an osmotic challenge. That is, changes in cell size are not predictive *a priori* of changes in cell fluidity under isotonic conditions. We conclude that cells in isotonic conditions exhibit a well-regulated (though temperature-dependent) fluidity that is little affected by variations in cell size as the cell cycle progresses. (Note that the same conclusion was obtained by Miyaoka *et al.* by using growth-arrested fibroblasts in the attached state.[50]) Nevertheless, this parameter can be strongly modulated by osmotic challenge, which induces a change in cytoskeletal friction caused not only by volumetric change but also induced by (de)polymerization of the actin cytoskeleton.[51,52]

Previous reports exist of extracellular media osmolarity modulating cell stiffness (*e.g.*,[53]) but, to our knowledge, fluidity modulation has not been reported previously. (Some studies have modeled cell viscoelasticity with springs and dashpots rather than as a power-law material. We note that the use of spring–dashpot viscoelastic models can be problematic;[6,10,28] when applied to creep deformation of cells, they predict a

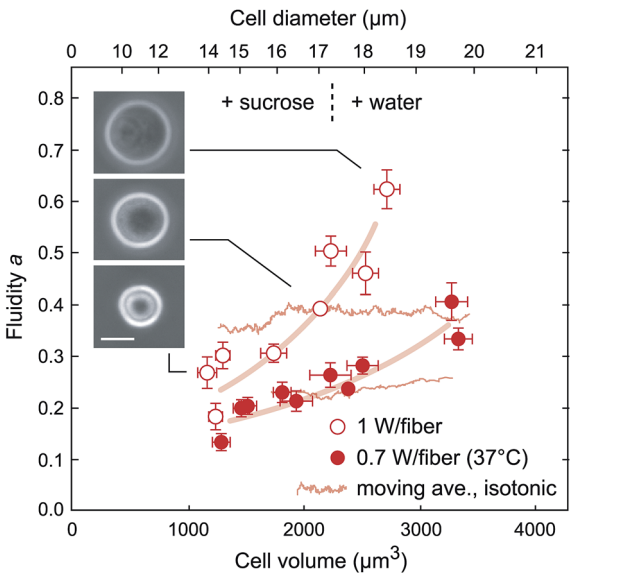

Fig. 7 Osmotic challenges alter fluidity by inducing cell swelling and shrinking in hypotonic and hypertonic media, respectively ($n = 11–399$ cells per point). Images show typical cell appearance with phase contrast microscopy (scale bar = 10 μm). Moving averages of fluidity *vs.* cell size show that no fluidity dependence on cell size (or on cell cycle position) is detectable in isotonic media.

relaxation time constant that appears to be an artifact of experiment duration.) In particular, fluidity changes were not detected in a study of hypertonic challenges applied to attached cells.[32] It is not yet clear whether the difference in results is related to the contrast between attached and suspended cells, or our approach of measuring fluidity independently of stiffness (in the earlier report, fluidity—power-law-exponent—was fit to a stiffness-frequency relationship, where stiffness was simultaneously strongly affected by osmolarity), or our additional inclusion of hypotonic conditions that produced relatively larger changes in fluidity, or a combination of these. Further work in this area might include identification of coupled changes in stiffness, which would require characterization of the refractive index of each cell. Such characterization was beyond the scope of our fluidity-centered investigation, but could be accomplished by, for example, integrating refractometry capability into the optical stretcher.

IV. Implications and outlook

Our goals in this study were to identify unambiguous fluidity modulators in the suspended state (in comparison to the attached state), and in general to provide experimental data to motivate continued development of predictive models of cell rheology and to accelerate development of mechanical flow cytometry techniques. We briefly discuss these topics here.

Which chemoenvironmental conditions most strongly modulate fluidity in relevant cell states?

A crucial question is whether the abundance of data collected from cells on stiff substrata (and thus frequently exhibiting focal adhesions, stress fibers, and associated internal tension, or "prestress") applies in the suspended state that is the milieu of high-throughput sorting. Previously we have found—in the context of human mesenchymal stem cells and their multipotency and mechanics during *in vitro* culture expansion—that prominent and dynamic mechanical markers in the attached state can be undetectable in the suspended state when they are manifested primarily by stress fiber presentation.[28] We have used a spectrum of pharmacological challenges to quickly identify relatively large changes in fluidity (and have found the strongest in latrunculin, quantified by its dose dependence). We do not claim that fluidity is unaltered by the other pharmacological challenges (ESI†), only that such alteration is considerably less than that for latrunculin at the dosages considered. In particular, the minimal influence of myosin inhibition and ATP depletion[17] in the suspended state shows that active contraction can be interrupted in the suspended (adherent or nonadherent) cell for tens of minutes, at least, without a detectable change in fluidity. This behavior differs from that noted for attached cells, in which actomyosin contraction manifested in stress fibers has been found to modulate prestress, which in turn strongly couples to fluidity magnitude.[54,55] The contrast emphasizes certain differences between attached- and suspended-cell mechanics that demand attention when considering high-throughput mechanical flow cytometry of suspended cells. To summarize our other findings, for the cells and conditions considered, fluidity also does not change detectably in response to pH changes over 6.5 to 8.5. However, it does decrease upon chemical fixation;[17] it increases with increasing temperature from 25 °C past 37 °C, as is also seen in attached cells[55] (and with no corresponding change in cell size); and it increases and decreases, respectively, with swelling and shrinking in the osmotically challenged cell.

How do these findings inform models of cells as soft matter?

Although our fluidity measurements are independent of any phenomenological model of cell mechanics, the results can be related to two models: the soft glassy rheology model[25] and the glassy wormlike chain model.[26] (The first connects fluidity to an athermal agitation energy that drives deformation and rearrangement; the second, to the reciprocal of the height of energy barriers blocking relaxation.) For example, our results are compatible with the prediction of both models that stiffness and fluidity are related by a large frequency ω_{inv} that derives from the kinetics of relaxation mechanisms. At lower frequencies, measured stiffness pivots around this point as a function of fluidity (Fig. 5(e)).[25] We have also found useful the physical interpretation that fluidity is inversely related to a measure of polymeric chain stickiness (*i.e.*, intracellular friction),[26] and recommend this interpretation as one that is compatible with our findings of altered fluidity upon cytoskeletal fixation, (dis)assembly, and/or swelling or shrinking by pharmacological or osmotic means.

Note, however, that some puzzles remain when comparing model to experiment. The first is the temperature dependence of fluidity. The soft glassy rheology model does not address molecular mechanisms, dealing more broadly with the class of soft matter that tends to deform by agitation-driven rearrangement; in fact, thermal energy is assumed to be negligible compared to jostling from neighboring regions. No explicit dependence on material temperature is provided to predict or explain the clear increase in fluidity with increasing temperature (Fig. 3(a)). The glassy wormlike chain model postulates that $a \approx 3\ kT/E_b$ for typical experimental conditions of $\omega \ll \omega_{inv}$, where k is Boltzmann's constant and E_b is interpreted as a characteristic energy barrier height.[26,56] A fluidity value of $a \approx 0.25$ at 37 °C therefore suggests $E_b \approx 0.3$ eV. However, our finding of $da/dT = 0.013\ ^\circ C^{-1}$ indicates $E_b \approx 0.02$ eV (ignoring any temperature dependence of E_b), an order-of-magnitude difference. The resolution may lie in recognizing that the fluidity *vs.* temperature relationship shown in Fig. 3(a) is an affine relationship, and in adapting a temperature offset so that $a \approx 3k(T - T_0)/E_b$, reminiscent of the empirical Vogel–Fulcher–Tammann law used to describe glass formation[57] (A. Kramer, personal communication). Here, T_0 can be interpreted as the temperature at which the cells behave like an elastic solid; the numerical difference mentioned above largely disappears if T_0 lies between the freezing point of water and room temperature.

The second puzzling area is the origin of the invariant angular frequency ω_{inv} that provides the only timescale in power-law rheology. This frequency has been associated with

water relaxation frequencies, though experimental reports have ranged over many orders of magnitude.[6,21,37,39] While we cannot yet reconcile different reports, our contribution has been to use bootstrapping to construct a confidence interval for this point for latrunculin action in suspended lymphoma cells, with fluidity measured independently from stiffness *via* optical stretching. Frustratingly, the invariant point lies within another deformation regime (Fig. 1 and 5(e)) and consequently must be extrapolated. However, another invariant stiffness has been achieved in practice by employing hyperosmotic conditions to compress the cell and inhibit cytoskeletal relaxation.[32] Determination of whether these invariant values are related, and how they emerge from molecular mechanisms, will be an exciting aspect of upcoming cytoskeletal mechanics research.

What do these results imply for mechanical flow cytometry?

Oscillatory optical stretching (OOS) presents advantages and disadvantages. Optical stretching fully decouples cell mechanics from cell size and transmembrane adhesion while interrogating single cells in the suspended state, a configuration expected to be crucial for high-throughput sorting. In optical stretching, cells are suspended in unfocused counter-propagating laser beams that create a distributed surface stress that can be nearly independent of cell size, especially compared to techniques that force a size-disperse population of cells through a smaller, fixed-size constriction. Additionally, OOS provides independent measurements of fluidity and stiffness to characterize single-cell viscoelasticity. Oscillatory capability avoids the need to drop data points from cells that have rotated during creep compliance experiments, and is further shown here to provide low-error mechanical data within one second of deformation, with fitting error that is still low compared to intrinsic cell-to-cell heterogeneity. However, the corresponding throughput is far smaller than reasonable flow cytometry rates of thousands of cells per second.

Some structural anisotropy remains in the suspended state, even if cell polarization and stress fibers are not observed (see Fig. S6 in ESI† for visualization of spatial heterogeneity involving the nucleus). This anisotropy conceivably contributes to the dispersion of mechanical parameters observed when measuring multiple whole cells (*e.g.*, the intrinsic standard deviation of 0.09 when measuring the fluidity of CH27 lymphoma cells, as shown in Fig. 3 (e, inset)). However, it is not at present possible to examine or quantify the effect of this variation on fluidity. Optical stretching is similar to fluorescence cytometry in this regard, in that—despite internal heterogeneity that could result in orientation dependence of mechanics and fluorescence, respectively—analysis and decision-making proceed even though each cell is measured only once and in a single orientation.

Additionally, optical stretching is not at this point capable of deforming cells in either the nonlinear power-law rheology regime or the poroelastic regime, both of which may feature interesting and leveragable differences between cell subpopulations or disease states. Therefore, although OOS provides sensitive mechanical characterization of suspended cell deformation down to ~10 nm, the technique is not now capable of detecting subpopulation rheological differences that manifest themselves only in other deformation regimes. Nevertheless, the current findings inform the mechanical dispersion of whole-cell fluidity and stiffness that can be expected in the suspended state, as is required to design other higher-throughput experimental approaches to detect and sort cell subpopulations based on mechanical signatures.

Acknowledgements

This work was supported by the Singapore-MIT Alliance for Research and Technology (SMART) Centre (BioSyM IRG). We gratefully acknowledge guidance from J. Guck *et al.* (Cambridge University and Technical University of Dresden) on optical stretcher construction. We appreciate helpful discussions with A. Kramer and K. Kroy (University of Leipzig) on interpreting fluidity measurements by using the glassy wormlike chain model, and the donation of CH27 lymphoma cells by S. H. Um and D. J. Irvine (MIT).

References

1 D. Chen, Q. Wen, P. Janmey, J. Crocker and A. Yodh, Rheology of soft materials, *Condens. Matter Phys.*, 2010, **1**, 301–322.
2 P. Kollmannsberger and B. Fabry, Linear and nonlinear rheology of living cells, *Annu. Rev. Mater. Res.*, 2011, **41**(1), 75–97.
3 S. C. Hur, N. K. Henderson-MacLennan, E. R. McCabe and D. Di Carlo, Deformability-based cell classification and enrichment using inertial microfluidics, *Lab Chip*, 2011, **11**(5), 912–920.
4 D. R. Gossett, T. Henry, S. A. Lee, Y. Ying, A. G. Lindgren, O. O. Yang, J. Rao, A. T. Clark and D. Di Carlo, Hydrodynamic stretching of single cells for large population mechanical phenotyping, *Proc. Natl. Acad. Sci. U. S. A.*, 2012, **109**(20), 7630–7635.
5 S. Byun, S. Son, D. Amodei, N. Cermak, J. Shaw, J. Kang, V. Hecht, M. Winslow, T. Jacks, P. Mallick and S. Manalis, Characterizing deformability and surface friction of cancer cells, *Proc. Natl. Acad. Sci. U. S. A.*, 2013, **110**(19), 7580–7585.
6 B. Fabry, G. Maksym, J. Butler, M. Glogauer, D. Navajas, N. Taback, E. Millet and J. Fredberg, Time scale and other invariants of integrative mechanical behavior in living cells, *Phys. Rev. E: Stat., Nonlinear, Soft Matter Phys.*, 2003, **68**(4), 41914.
7 G. Lenormand, E. Millet, B. Fabry, J. Butler and J. Fredberg, Linearity and time-scale invariance of the creep function in living cells, *J. R. Soc., Interface*, 2004, **1**(1), 91–97.
8 N. Desprat, A. Richert, J. Simeon and A. Asnacios, Creep function of a single living cell, *Biophys. J.*, 2005, **88**(3), 2224–2233.
9 M. Balland, N. Desprat, D. Icard, S. Féréol, A. Asnacios, J. Browaeys, S. Hénon and F. Gallet, Power laws in microrheology experiments on living cells: comparative

analysis and modeling, *Phys. Rev. E: Stat., Nonlinear, Soft Matter Phys.*, 2006, **74**(2), 21911.

10 P. Roca-Cusachs, I. Almendros, R. Sunyer, N. Gavara, R. Farré and D. Navajas, Rheology of passive and adhesion-activated neutrophils probed by atomic force microscopy, *Biophys. J.*, 2006, **91**(9), 3508–3518.

11 B. Hoffman, G. Massiera, K. Van Citters and J. Crocker, The consensus mechanics of cultured mammalian cells, *Proc. Natl. Acad. Sci. U. S. A.*, 2006, **103**(27), 10259.

12 J. Hemmer, J. Nagatomi, S. Wood, A. Vertegel, D. Dean and M. LaBerge, Role of cytoskeletal components in stress-relaxation behavior of adherent vascular smooth muscle cells, *J. Biomech. Eng.*, 2009, **131**(4), 041001.

13 E. Zhou, S. Quek and C. Lim, Power-law rheology analysis of cells undergoing micropipette aspiration, *Biomech. Model. Mechanobiol.*, 2010, **9**(5), 1–10.

14 E. Moeendarbary, L. Valon, M. Fritzsche, A. R. Harris, D. A. Moulding, A. J. Thrasher, E. Stride, L. Mahadevan and G. T. Charras, The cytoplasm of living cells behaves as a poroelastic material, *Nat. Mater.*, 2013, **12**(3), 253–261.

15 P. Fernández, P. Pullarkat and A. Ott, A master relation defines the nonlinear viscoelasticity of single fibroblasts, *Biophys. J.*, 2006, **90**(10), 3796–3805.

16 P. Fernández and A. Ott, Single cell mechanics:stress stiffening and kinematic hardening, *Phys. Rev. Lett.*, 2008, **100**(23), 238102.

17 J. M. Maloney, E. Lehnhardt, A. F. Long and K. J. Van Vliet, Mechanical fluidity of fully suspended biological cells, *Biophys. J.*, 2013, **105**(8), 1767–1777.

18 D. Robert, T.-H. Nguyen, F. Gallet and C. Wilhelm, In vivo determination of fluctuating forces during endosome trafficking using a combination of active and passive microrheology, *PLoS One*, 2010, **5**(4), e10046.

19 J. Fredberg and B. Fabry, The cytoskeleton as a soft glassy material, in *Models and Measurements in Cell Mechanics*, ed. M. Mofrad and R. Kamm, Cambridge University Press: Cambridge UK, 2006, ch. 3, pp. 50–70.

20 F. J. Alenghat, B. Fabry, K. Y. Tsai, W. H. Goldmann and D. E. Ingber, Analysis of cell mechanics in single vinculin-deficient cells using a magnetic tweezer, *Biochem. Biophys. Res. Commun.*, 2000, **277**(1), 93–99.

21 M. Puig-de Morales, E. Millet, B. Fabry, D. Navajas, N. Wang, J. Butler and J. Fredberg, Cytoskeletal mechanics in the adherent human airway smooth muscle cell: probe specificity and scaling of protein-protein dynamics, *Am. J. Physiol.: Cell Physiol.*, 2004, **287**(3), C643–C654.

22 S. Hiratsuka, Y. Mizutani, M. Tsuchiya, K. Kawahara, H. Tokumoto and T. Okajima, The number distribution of complex shear modulus of single cells measured by atomic force microscopy, *Ultramicroscopy*, 2009, **109**(8), 937–941.

23 J. M. Maloney and K. J. Van Vliet, On the origin and extent of mechanical variation among cells, arXiv preprint arXiv:1104.0702, 2011.

24 P. Cai, Y. Mizutani, M. Tsuchiya, J. M. Maloney, B. Fabry, K. J. Van Vliet and T. Okajima, Quantifying cell-to-cell variation in power-law rheology, *Biophys. J.*, 2013, **105**(5), 1093–1102.

25 P. Sollich, Rheological constitutive equation for a model of soft glassy materials, *Phys. Rev. E: Stat., Nonlinear, Soft Matter Phys.*, 1998, **58**(1), 738–759.

26 K. Kroy and J. Glaser, The glassy wormlike chain, *New J. Phys.*, 2007, **9**, 416.

27 J. Guck, S. Schinkinger, B. Lincoln, F. Wottawah, S. Ebert, M. Romeyke, D. Lenz, H. Erickson, R. Ananthakrishnan, D. Mitchell, *et al.*, Optical deformability as an inherent cell marker for testing malignant transformation and metastatic competence, *Biophys. J.*, 2005, **88**(5), 3689–3698.

28 J. M. Maloney, D. Nikova, F. Lautenschläger, R. Langer, J. Guck and K. J. Van Vliet, Mesenchymal stem cell mechanics from the attached to the suspended state, *Biophys. J.*, 2010, **99**(8), 2479–2487.

29 G. Haughton, L. W. Arnold, G. A. Bishop and T. J. Mercolino, The CH series of murine B cell lymphomas: neoplastic analogues of Ly-1+ normal B cells, *Immunol. Rev.*, 1986, **93**(1), 35–52.

30 R. Barer and S. Tkaczyk, Refractive index of concentrated protein solutions, *Nature*, 1954, **173**(4409), 821–822.

31 J. A. Thomas, R. N. Buchsbaum, A. Zimniak and E. Racker, Intracellular pH measurements in Ehrlich ascites tumor cells utilizing spectroscopic probes generated in situ, *Biochemistry*, 1979, **18**(11), 2210–2218.

32 E. Zhou, X. Trepat, C. Park, G. Lenormand, M. Oliver, S. Mijailovich, C. Hardin, D. Weitz, J. Butler and J. Fredberg, Universal behavior of the osmotically compressed cell and its analogy to the colloidal glass transition, *Proc. Natl. Acad. Sci. U. S. A.*, 2009, **106**(26), 10632–10637.

33 J. Guck, R. Ananthakrishnan, H. Mahmood, T. Moon, C. Cunningham and J. Käs, The optical stretcher: a novel laser tool to micromanipulate cells, *Biophys. J.*, 2001, **81**(2), 767–784.

34 B. Lincoln, S. Schinkinger, K. Travis, F. Wottawah, S. Ebert, F. Sauer and J. Guck, Reconfigurable microfluidic integration of a dual-beam laser trap with biomedical applications, *Biomed. Microdevices*, 2007, **9**(5), 703–710.

35 M. H. Kutner, C. Nachtsheim and J. Neter, *Applied Linear Regression Models*, McGraw-Hill/Irwin, 2004.

36 M. Chernick, *Bootstrap Methods: A Practitioner's Guide*, Wiley, New York, 1999.

37 G. Lenormand, E. Millet, C. Park, C. Hardin, J. Butler, N. Moldovan and J. Fredberg, Dynamics of the cytoskeleton: how much does water matter?, *Phys. Rev. E: Stat., Nonlinear, Soft Matter Phys.*, 2011, **83**(6), 061918.

38 M. Coué, S. L. Brenner, I. Spector and E. D. Korn, Inhibition of actin polymerization by latrunculin A, *FEBS Lett.*, 1987, **213**(2), 316–318.

39 R. Laudadio, E. Millet, B. Fabry, S. An, J. Butler and J. Fredberg, Rat airway smooth muscle cell during actin modulation: rheology and glassy dynamics, *Am. J. Physiol.: Cell Physiol.*, 2005, **289**(6), C1388–C1395.

40 C. Rotsch and M. Radmacher, Drug-induced changes of cytoskeletal structure and mechanics in fibroblasts: an atomic force microscopy study, *Biophys. J.*, 2000, **78**(1), 520–535.

41 T. Wakatsuki, B. Schwab, N. C. Thompson and E. L. Elson, Effects of cytochalasin D and latrunculin B on mechanical properties of cells, *J. Cell Sci.*, 2001, **114**(5), 1025–1036.
42 L. A. MacQueen, M. Thibault, M. D. Buschmann and M. R. Wertheimer, Electromechanical deformation of mammalian cells in suspension depends on their cortical actin thicknesses, *J. Biomech.*, 2012, **45**(16), 2797–2803.
43 S. Yamada, D. Wirtz and S. C. Kuo, Mechanics of living cells measured by laser tracking microrheology, *Biophys. J.*, 2000, **78**(4), 1736–1747.
44 K. Van Citters, B. Hoffman, G. Massiera and J. Crocker, The role of F-actin and myosin in epithelial cell rheology, *Biophys. J.*, 2006, **91**(10), 3946–3956.
45 D. Ellis and R. Thomas, Direct measurement of the intracellular pH of mammalian cardiac muscle, *J. Phys.*, 1976, **262**(3), 755–771.
46 C. Aickin, Direct measurement of intracellular pH and buffering power in smooth muscle cells of guinea-pig vas deferens, *J. Phys.*, 1984, **349**(1), 571–585.
47 A. Tolkovsky and C. Richards, Na+/H+ exchange is the major mechanism of pH regulation in cultured sympathetic neurons: measurements in single cell bodies and neurites using a fluorescent pH indicator, *Neuroscience*, 1987, **22**(3), 1093–1102.
48 P. Sampath and T. D. Pollard, Effects of cytochalasin, phalloidin and pH on the elongation of actin filaments, *Biochemistry*, 1991, **30**(7), 1973–1980.
49 K. M. Schmoller, S. Köhler, A. H. Crevenna, R. Wedlich-Söldner and A. R. Bausch, Modulation of cross-linked actin networks by ph, *Soft Matter*, 2012, **8**(37), 9685–9690.
50 A. Miyaoka, Y. Mizutani, M. Tsuchiya, K. Kawahara and T. Okajima, Rheological properties of growth-arrested fibroblast cells under serum starvation measured by atomic force microscopy, *Jpn. J. Appl. Phys.*, 2011, **50**(8), 08LB16.
51 K. R. Hallows, C. H. Packman and P. A. Knauf, Acute cell volume changes in anisotonic media affect F-actin content of HL-60 cells, *Am. J. Physiol.: Cell Physiol.*, 1991, **261**(6), C1154–C1161.
52 F. Lang, G. L. Busch, M. Ritter, H. Völkl, S. Waldegger, E. Gulbins and D. Häussinger, Functional significance of cell volume regulatory mechanisms, *Phys. Rev.*, 1998, **78**(1), 247–306.
53 F. Guilak, G. R. Erickson and H. P. Ting-Beall, The effects of osmotic stress on the viscoelastic and physical properties of articular chondrocytes, *Biophys. J.*, 2002, **82**(2), 720–727.
54 D. Stamenović, B. Suki, B. Fabry, N. Wang, J. Fredberg and J. Buy, Rheology of airway smooth muscle cells is associated with cytoskeletal contractile stress, *J. Appl. Physiol.*, 2004, **96**(5), 1600–1605.
55 P. Bursac, G. Lenormand, B. Fabry, M. Oliver, D. Weitz, V. Viasnoff, J. Butler and J. Fredberg, Cytoskeletal remodelling and slow dynamics in the living cell, *Nat. Mater.*, 2005, **4**(7), 557–561.
56 C. Semmrich, T. Storz, J. Glaser, R. Merkel, A. Bausch and K. Kroy, Glass transition and rheological redundancy in F-actin solutions, *Proc. Natl. Acad. Sci. U. S. A.*, 2007, **104**(51), 20199.
57 C. A. Angell, Formation of glasses from liquids and biopolymers, *Science*, 1995, **267**(5206), 1924–1935.